Multi-Period OPF Model of Power Systems with HVDC Connected Intermittent Wind Power Generation

Abbas Rabiee, Alireza Soroudi

***Abstract*—This paper presents a model for a multi-period optimal power flow (MP-OPF) problem which includes offshore wind farm connected to the grid by line-commutated converter high-voltage DC (LCC-HVDC) link. The offshore wind farm is composed of doubly fed induction generators (DFIGs), and the DFIGs capability curve is considered in order to obtain a more realistic dispatch for wind farm. The uncertainties of wind power generation are also taken into account using a scenario based approach which can be adopted by system operator to obtain the optimal active and reactive power schedules for both thermal and renewable generating units. To illustrate the effectiveness of the proposed approach, it is applied on the IEEE 118-bus system. The obtained results demonstrate the capability of the proposed MP-OPF model for optimal operation of power system.**

***Index Terms*—HVDC, wind power, OPF, scenario modeling, uncertainty.**

NOMENCLATURE

t/s	t/s time interval and wind scenario index
k	Index of system buses
m	rectifier ($m=r$)/inverter ($m=i$)
v_{in}^{c}	Cut-in speed of wind turbine (m/s)
v_{out}^{c}	Cut-out speed of wind turbine (m/s)
v_{rated}	Rated speed of wind turbine (m/s)
UR_{G_k}	Ramp up limit of power generation of k-th thermal unit
DR_{G_k}	Ramp down limit of power generation of k-th thermal unit
$\lambda(s,t)$	Electricity price in scenario s and time t(\$/MW)
π_s	Probability of scenario s
$Pp(s,t)$	Power purchased from pool market in time t and scenario s
wp_s	Percent of available wind generation capacity in scenario s
P_{st}/Q_{st}	Active/reactive power of DFIG's stator
V_{st}/I_{st}	Stator voltage/current of DFIG
X_m/X_{st}	DFIG's mutual/stator reactance
sl	DFIG's rotor slip
δ	DFIG's load angle
I_{rt}	DFIG's rotor current
P_{rt}/Q_{rt}	Active/reactive power of DFIG's rotor
P_{wg}/Q_{wg}	Active/reactive power Output of DFIG
P_{wg}^{r}	Rated active power Output of DFIG
α_m	Ignition angle
$V_{d0,m}$	Ideal no-load voltage at the terminals
$V_{d,m}$	DC magnitudes of voltages at the terminals
B_m	Number of series-connected bridges in a terminal
T_m	Tap ratio of HVDC's transformer
V_m	effective voltage magnitudes at the AC terminals of HVDC
$R_{c,m}$	Commutation resistances
I_d	DC current carried by the HVDC link
$B_{sh,m}$	Shunt admittance of Passive filters at the AC side of HVDC terminals
$Q_{sh,m}$	Reactive power compensation at the AC side of HVDC terminals
$R_{L,d}$	Resistance of HVDC line
φ_m	Angle difference between the fundamental line current and line-to-neutral AC voltage
$P_{d,m}$	Active power flowing through HVDC link
Q_m	Reactive power flowing into HVDC link
	AC network's variables and parameters:
P_{G_k}/Q_{G_k}	Active/reactive power generation by thermal unit located in bus k
P_{L_k}/Q_{L_k}	Active/reactive load in bus k
V_k/θ_k	Voltage magnitude/angle in bus k
S_ℓ	Flow of ℓ-th transmission line
Y_{kj}/γ_{kj}	Magnitude/angle of kj-th element of admittance matrix

The authors are with the Young Researchers club, Science and Research Branch, Tehran, Iran Email: alireza.soroudi@gmail.com , abbas.rabiee@gmail.com .

I. INTRODUCTION

A. Motivation and Approach

UTILIZATION of wind power generation technology is taking substantial attention around the world due to the economical and environmental concerns [1]. The problem of uncertainty modeling of wind generation facilities is still an important issue [2]. Hence, the appropriate modeling of wind power generation in optimal power flow (OPF) formulation is essential. The ultimate goal of the system operator is operating the system in a way that the total operating cost is minimized for a given operating horizon while satisfying a set of technical constraints. Such an optimization problem is called multi-period optimal power flow (MP-OPF) [3]. Generally, the objective of a MP-OPF problem is to find the steady state operation point of power system which minimizes generation cost or maximizes the social welfare and loadability, while satisfying a set of technical constraints such as power flow equations, limits on generators' real and reactive powers, line flow limits and output of various compensating devices [4], [5].

In many countries, the best locations for onshore wind farms are already developed, and the utilities are turning to offshore sites. The main reason of this attraction is the availability of enormous wind resources. The lack of obstacles such as hills, and generally smooth surface of the sea, also make the wind generation more reliable. The offshore wind farm is generally located far away from the onshore grid. If the distance is long or if the offshore wind farm is connected to a weak AC onshore grid, a high-voltage DC

(HVDC) transmission system may be a more suitable choice than the conventional high-voltage AC transmission [6]. Two types of HVDC transmission topologies, i.e., HVDC with voltage source converter (VSC-HVDC) using insulated gate bipolar transistors (IGBTs) and line-commutated converter HVDC (LCC-HVDC) are used nowadays for offshore wind farm connectivity [7], [8].

B. Literature Review

Different OPF models have been proposed in the literature to consider the impacts of wind power generation. The objective functions cover a vast range of items such as :

- opportunity cost of wind power shortage & surplus [9]
- cost of environmental benefit loss [9]
- expected penalty cost for not using all available wind power [10]
- expected cost of calling up power reserves because of wind power shortage [10]
- risk due to expected energy not supplied (EEENS) and total operating costs [11]
- location marginal prices, and reserve costs [11]
- minimizing losses within the wind farm and the HVDC transmission system and maximizing production output [12]
- voltage regulation of the electrical grid to which farms are connected [13]

The proposed approaches for handling the uncertainty of wind power generation are summarized as follows: Monte Carlo [9], triangular approximate distribution (TAD) [11], scenario based modeling [14], [15].

C. Contributions

In this paper, a comprehensive model for MP-OPF is proposed, by including the uncertain wind power generation. The offshore wind farms are considered to be of doubly fed induction generator (DFIG) type. These farms are connected to the AC transmission system by LCC-HVDC links. Due to the importance of considering reactive power requirements of converters at both sides of the LCC-HVDC connection, capability curves of wind farm's DFIGs are also modeled. Considering the capability curves for DFIGs makes the generation schedule more realistic.

D. Paper Organization

This paper is set out as follows: Section II presents problem formulation. Simulation results are presented in Section III and finally, Section IV summarizes the findings of this work.

II. Problem formulation

Load flow equations of AC/DC networks, HVDC links steady state model and characteristics of wind power generation are formulated in this section. The assumptions, decision variables, constraints and objective function of the proposed MP-OPF are described as follows:

A. Decision Variables

The decision variables of the problem include: hourly generation schedule and terminal voltage of thermal units, tap settings of on-load tap changers and HVDC link transformers. These variables are determined based on a set of wind generation scenarios and remain the same for each scenario. These types of variables are called 'here and now' variables. On the other hand, there exist another set of variables which change with the scenarios like voltage of PQ buses, transmitted power by HVDC link and etc. These types of variables are called 'wait and see' variables [16].

B. Capability Curve of DGIFs

1) Stator current limit: this limit models the stator heating due to the stator winding Joule losses. By considering all quantities in per-unit (pu), the relation between stator voltage, current and active/reactive power outputs can be expressed as follows [12]:

$$P_{st}^2 + Q_{st}^2 = (V_{st} I_{st})^2 \tag{1}$$

2) Rotor current limit: This limit considers the rotor heating due to the rotor winding Joule losses. In pu, the equation of active and reactive power output of DFIG's stator is as follows [17]:

$$P_{st} = \frac{X_m}{X_{st}} V_{st} I_{rt} sin(\delta) \tag{2}$$

$$Q_{st} = \frac{X_m}{X_{st}} V_{st} I_{rt} cos(\delta) - \frac{V_{st}^2}{X_{st}} \tag{3}$$

$$P_{st}^2 + (Q_{st} + \frac{V_{st}^2}{X_{st}})^2 = (\frac{X_m}{X_{st}} V_{st} I_{rt})^2 \tag{4}$$

3) Steady state stability limit: The steady-state stability limit shows the maximum reactive power absorption by the DGIG, which is obtained as follows:

$$Q_{st} = -\frac{V_{st}^2}{X_{st}} \tag{5}$$

Equation (5) gives a vertical line at $[-\frac{V_{st}^2}{X_{st}}, 0]$, in P-Q plane. It is noteworthy that $\frac{V_{st}^2}{X_{st}}$ is the no-load reactive power absorption, which means that the DFIG becomes unstable when the reactive power consumption is greater than the no-load reactive power [12].

4) Total Capability limit $(sl_{\min} \leq sl \leq 0)$*:* The rotor active-power generation, neglecting stator and rotor resistance, can be expressed as follows:

$$P_{rt} = -sl * P_{st} \tag{6}$$

The grid-side inverter of the DFIG is usually operating with a unity power factor [12]. Hence, the injected power from the rotor is zero, and total reactive power output of DFIG is as follows:

$$Q_{rt} = 0 \tag{7}$$

The DFIG's total active and reactive power generations are obtained by adding rotor active/reactive powers to the stator active/reactive powers, as follows:

$$P_{wg} = P_{st} + P_{rt} = (1 - sl) P_{st} \tag{8}$$

$$Q_{ws} = Q_{st} + Q_{rt} = Q_{st} \tag{9}$$

By defining:

$$A = I_{st,\max}; B = \frac{1}{(1 - sl_{\min})^2}; C = \frac{X_m}{X_{st}} I_{rt,\max}$$

The maximum/minimum limits of reactive power output of DFIG are expressed as follows:

$$Q_{g,\max}^{(1)} = +\sqrt{(AV_{st})^2 - BP_{wg}^2} \tag{10}$$

$$Q_{g,\max}^{(2)} = +\sqrt{(CV_{st})^2 - BP_{wg}^2} - \frac{V_{st}^2}{X_{st}} \tag{11}$$

$$Q_{g,\max} = \min(Q_{g,\max}^{(1)}, Q_{g,\max}^{(2)}) \tag{12}$$

$$Q_{g,\min}^{(1)} = -\frac{V_{st}^2}{X_{st}} \tag{13}$$

$$Q_{g,\min}^{(2)} = -\sqrt{(AV_{st})^2 - BP_{wg}^2} \tag{14}$$

$$Q_{g,\min} = \max(Q_{g,\min}^{(1)}, Q_{g,\min}^{(2)}) \tag{15}$$

5) Wind-Turbine maximum/minimum active power output limit: The restrictions related to the maximum active power available at wind turbine, are expressed as follows:

$$0 \leq P_{wg} \leq wp_s * P_{wg}^r \tag{16}$$

The capability curve of the DFIG determines the feasible operation regime in P-Q plane [17] as shown in Fig.1. From this figure, the feasible operating area in P-Q plain, is the area specified by $(z_1, z_2, z_3, z_4, z_5, z_6)$ coordinates.

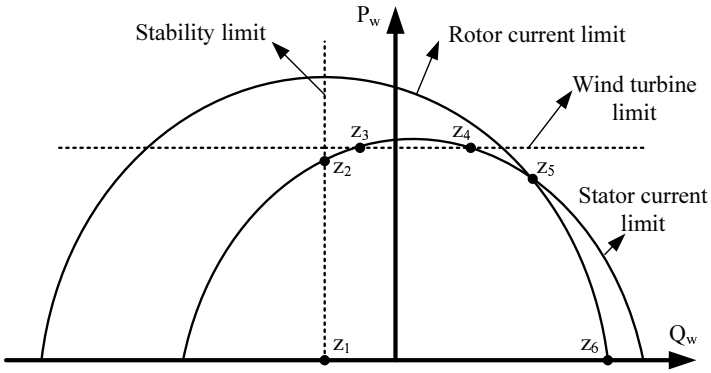

Fig. 1. Capability curve of DFIG

C. HVDC Modeling

Load flow equations of the LCC-HVDC system are as follows. The schematic of the LCC-HVDC link is depicted in Fig. 2.

For $m = r$, i (r: Rectifier, i: Inverter):

$$V_{d0,m} = \frac{3\sqrt{2}}{\pi} B_m T_m V_m \tag{17}$$

$$V_{d,m} = V_{d0,m} cos(\alpha_m) - B_m R_{c,m} I_d \tag{18}$$

$$I_d = \frac{V_{d,r} - V_{d,i}}{R_{L,d}} \tag{19}$$

$$cos(\varphi_m) = \frac{V_{d,m}}{V_{d0,m}} \tag{20}$$

$$P_{d,m} = V_{d,m} I_d \tag{21}$$

$$Q_m = P_{d,m} tan(\varphi_m) \tag{22}$$

D. Uncertainty Modeling of Wind Power Generation

In this paper, a scenario based model is used to describe the wind power generation [18]. It is assumed that the probability density function of wind speed as well as the characteristic curve of wind turbine is available. Using these data and scenario generation technique (described in Appendix B) the wind power generation is described and modeled in the proposed MP-OPF model.

E. Load Flow Equations of AC Network

The AC load flow equations for $k-th$ bus, is as follows:

$$P_{G_k}(t) - P_{L_k}(t) = P_k(s,t) \tag{23}$$

$$Q_{G_k}(s,t) - Q_{L_k}(t) = Q_k(s,t) \tag{24}$$

where, $P_k(s,t)$ and $Q_k(s,t)$ are injected active and reactive powers, respectively, which are calculated as follows:

$$P_k(s,t) = \sum_{j=1}^{NB} V_k(s,t) V_j(s,t) Y_{kj} cos(\theta_k(s,t) - \theta_j(s,t) - \gamma_{kj}) \tag{25}$$

$$Q_k(s,t) = \sum_{j=1}^{NB} V_k(s,t) V_j(s,t) Y_{kj} sin(\theta_k(s,t) - \theta_j(s,t) - \gamma_{kj}) \tag{26}$$

The magnitude of voltage in each bus k should remain between the safe operating limits during each scenario s and time t:

$$V_k^{min} \leq V_k(s,t) \leq V_k^{max} \tag{27}$$

Also, the flow of transmission lines must be below their corresponding limits:

$$|S_\ell(s,t)| \leq S_\ell^{max} \tag{28}$$

F. Load Flow Equations at the Interface of AC/DC Networks

According to Fig. 2, at the inverter side of the HVDC connection (i.e. for $k = i$), the power balance equations of AC/DC networks are as follows:

$$P_i(s,t) = P_{G_i}(t) + P_{d,i}(s,t) - P_{L_i}(t) \tag{29}$$

$$Q_i(s,t) = Q_{G_i}(t) + B_{sh,i} V_i^2(s,t) + Q_{sh,i}(s,t) - Q_{d,i}(s,t) - Q_{L_i}(t) \tag{30}$$

Similarly, for the rectifier side (i.e. for $k = r$), by neglecting the active power losses of the transformers connecting the WF to HVDC rectifier terminal, the power balance equations of AC/DC networks are as follows:

$$P_{wg}(s,t) = P_{d,r}(s,t) \tag{31}$$

$$Q_{wg}^{HV}(s,t) + B_{sh,r} V_r^2(s,t) + Q_{sh,r}(s,t) = Q_{d,r}(s,t) \tag{32}$$

where, $Q_{wg}^{HV}(s,t)$ is total reactive power injected from the HV side of transformers connecting the WF to the HVDC link, in scenario s and time t. It is worth to note that passive filters are also connected to the HVDC rectifier and inverter terminals, which are represented by constant shunt admittance in (30) and (32).

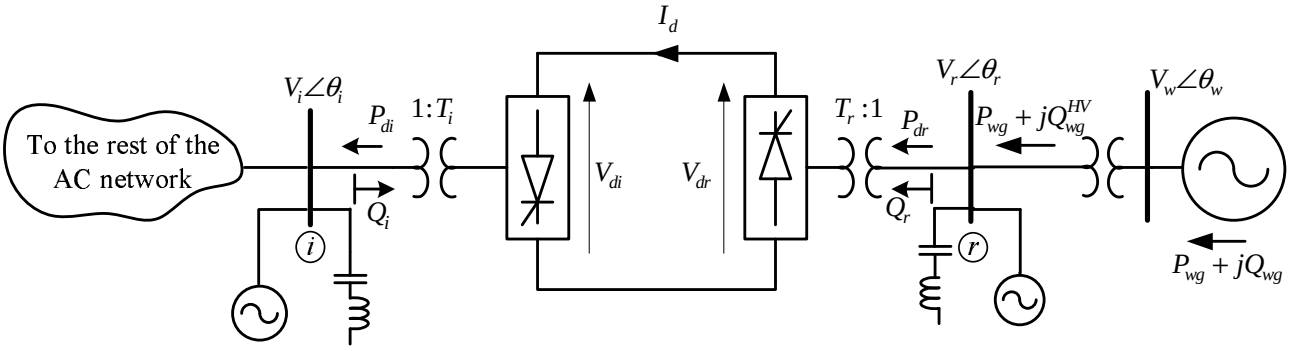

Fig. 2. One-line diagram of wind farm connection using LLC-HVDC link

G. Thermal Generation Constraints

The following constraints are considered in order to model the cost and technical limits of thermal generation units [19]:

1) Total production cost of thermal units: the production cost of thermal units is defined as:

$$F_{k,t}(P_{G_k}(t)) = a_k P_{G_k}^2(t) + b_k P_{G_k}(t) + c_k \quad (33)$$

where a_k, b_k and c_k are the fuel cost coefficients of the k-th generation unit.

2) Generation limits of thermal units:

$$P_{G_k}^{min} \le P_{G_k}(t) \le P_{G_k}^{max} \quad (34)$$
$$Q_{G_k}^{min} \le Q_{G_k}(t) \le Q_{G_k}^{max} \quad (35)$$

where $P_{G_k}^{max/min}$ and $Q_{G_k}^{max/min}$ are the maximum/minimum limits of active/reactive power outputs in k-th thermal unit.

3) Ramp up and ramp down constraints: the output power change rate of the thermal unit should be below the pre-specified limits called ramp rates. This is to avoid damaging the boiler and combustion equipments. These limits are stated as follows:

$$P_{G_k}(t) \ge P_{G_k}(t-1) - DR_{G_k} \quad (36)$$
$$P_{G_k}(t) \le P_{G_k}(t-1) + UR_{G_k} \quad (37)$$

where UR_{G_k} and DR_{G_k} are the ramp up/down limits of the k-th thermal unit (MW/h).

H. Objective function

The objective function of MP-OPF to be minimized is defined as the total cost paid by the retailer and is calculated as follows:

$$TC = \sum_{s,t}(\pi_s Pp(s,t)\lambda(s,t)) + \sum_{k,t} F_{k,t}(P_{G_k}(t)) \quad (38)$$

where $Pp(s,t)$ is the purchased power from the pool market in time t and scenario s.

III. Simulation results

The proposed probabilistic model for the MP-OPF problem is examined on the IEEE 118-bus test system. This system consists of 54 generator buses, and 186 transmission lines. The data of generating units along with the voltage limits and transmission lines flow limits are given in [20]. The purchased power from pool market is injected to the network through slack bus which is B_{69} in this network. Also, electricity price in scenario s and time t, i.e. $\lambda(s,t)$, is assumed to be even during the operating horizon and equal to 8 \$/h.

In this study, two wind farms (WFs) are considered. Each WF consists of 500 DFIG-based wind turbine. The characteristics of wind turbine are given in Table I. Hence, the total capacity of each WF is 1000 MW which is connected to the system via a 24-pulse LLC-HVDC link. HVDC links are bipolar with the rating of 1000 MW, and ± 250 kV. The data of these DC links are derived from [21], and are given in Table VI. As it is shown in Fig. 6, WF-1 and WF-2 are connected to buses B_{10} and B_{80}, respectively.

For the sake of brevity, three load levels ($T_{1\to 3}$) are considered for each day as 90%, 100% and 80% of the peak value. This multi-period load curve is depicted in Fig.3 . Also, it is assumed

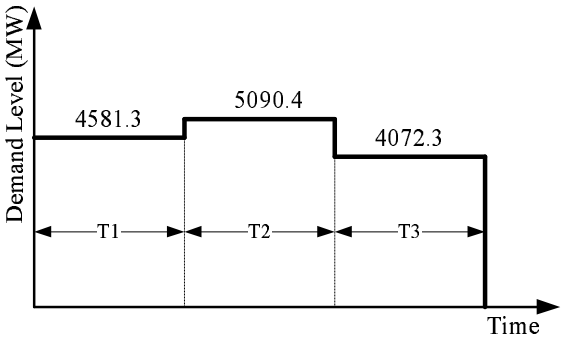

Fig. 3. Demand level values in different time intervals

that the total load of each period is distributed based on the initial load share of each bus, as given in [20].

Using the technique described in Appendix B, 12 scenarios are determined for each WF which are given in Table IV. The proposed algorithm is implemented in General Algebraic Modeling System (GAMS) [22] environment and solved by CONOPT solver [23].

Optimal active power generation schedules and voltage magnitude of generation buses, for all intervals are given in Figs. 4, 5, respectively. As mentioned earlier, these variables are 'here and now' control variables and the obtained optimal schedules for these variables are the same for all scenarios. The total cost of thermal generation units is equal to 161704.554 \$, whereas the cost paid for power procurement from pool market is equal to 4242.288 \$. The tap settings of transformers at both sides of the HVDC links, which are also 'here and now' control variables, are given in Table II, for all time intervals.

Table III gives the optimal schedule of HVDC links for all

TABLE I
THE TECHNICAL CHARACTERISTICS OF WIND TURBINES

v_{in}^{c} (m/s)	v_{rated} (m/s)	v_{out}^{c} (m/s)	X_m (pu)	X_{st} (pu)	sl_{min}	$I_{rt,max}$ (pu)	$I_{st,max}$ (pu)	P_{wg}^{r} (MW)
4	14	25	2.7891	2.8421	-0.3000	1.3893	1.0500	2.0000

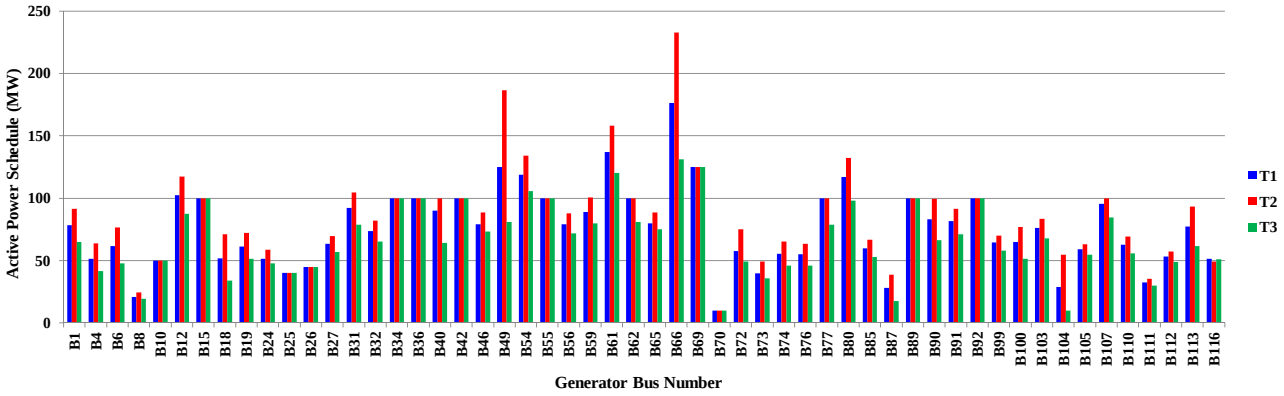

Fig. 4. Active power schedule of thermal generation units

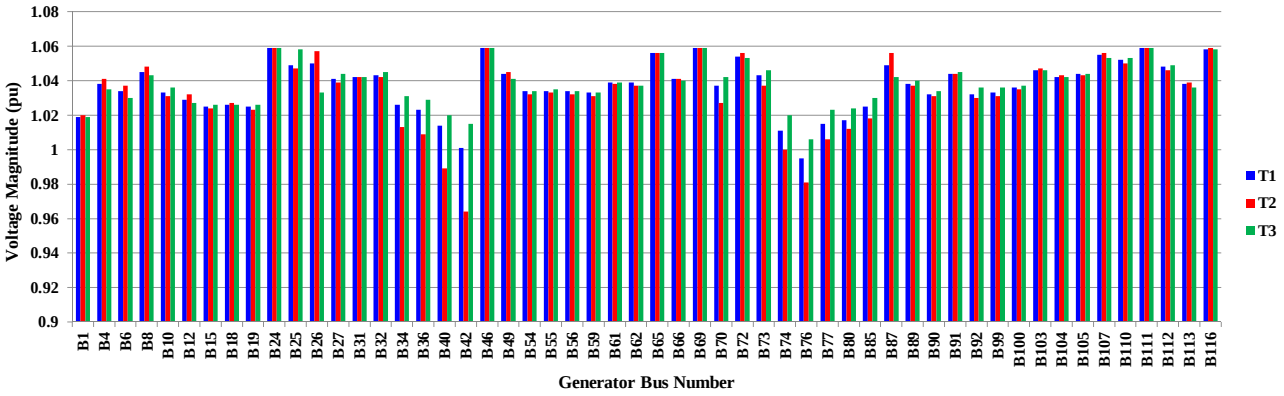

Fig. 5. Optimal voltage magnitude generation buses

scenarios in the studied horizon. for the sake of briefness, only the schedules of scenarios $s_1 - s_6$ are given in this table. It is observed from this table that $HVDC_1$ is loaded lightly, in comparison to $HVDC_2$. This is due to the capacity limit of the transmission line L_9, (between buses B_{10} and B_9), which connects bus B_{10} to the AC network. But, for $HVDC_2$, bus B_{80} is connected to the system by several transmission lines (i.e. the lines L_{123}, L_{124}, L_{125}, L_{127}, L_{148}, L_{151}, L_{152} and L_{153}), and hence, sufficient capacity is available for transmission of generated power of WF-2. Also, active and reactive power generation of WF-1 and WF-2 for all wind scenarios in the studied horizon, are provided in Table V.

TABLE II
THE TAP SETTINGS OF HVDC LINKS

Link#	Time interval	Inverter	Rectifier
$HVDC_1$	T_1	0.450	0.456
	T_2	0.451	0.476
	T_3	0.449	0.476
$HVDC_2$	T_1	0.460	0.493
	T_2	0.462	0.489
	T_3	0.456	0.475

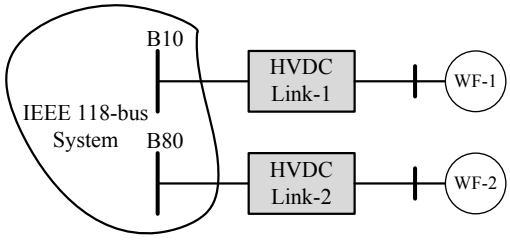

Fig. 6. The schematic of the system under study

IV. CONCLUSION

This paper presents a comprehensive multi-period optimal power flow (MP-OPF) model which describes a power system with uncertain wind power injections through LCC-HVDC links. The objective function of this MP-OPF is defined as minimizing the operating cost of the system in the presence of intermittent renewable energy resources like wind farms (WFs). Scenario based approach is utilized to model the uncertainty of wind power generation. One of the features of the proposed MP-OPF is to schedule both 'here and now' and 'wait and see' control

TABLE III
THE SCHEDULES OF HVDC LINK VARIABLES

			φ_r (Radian)	φ_i (Radian)	α_r (Radian)	α_i (Radian)	$V_{d,r}$ (kV)	$V_{d,i}$ (kV)	$P_{d,r}$ (MW)	$P_{d,i}$ (MW)	$Q_{d,r}$ (MVAr)	$Q_{d,i}$ (MVAr)	I_d (kA)	V_r (kV)	V_i (kV)
$HVDC_1$	s_1	T_1	0.35	0.09	0.35	0.09	550.00	549.81	5.23	5.23	1.92	0.48	0.01	233.20	227.13
	s_1	T_2	0.17	0.18	0.08	0.09	550.00	544.65	147.02	145.59	25.48	25.74	0.27	216.98	227.06
	s_1	T_3	0.18	0.18	0.08	0.09	550.00	544.34	155.56	153.96	27.58	27.88	0.28	217.28	228.08
	s_2	T_1	0.35	0.35	0.35	0.35	518.62	518.41	5.23	5.23	1.92	1.92	0.01	219.90	227.13
	s_2	T_2	0.17	0.18	0.08	0.09	550.00	544.65	147.02	145.59	25.48	25.74	0.27	216.98	227.06
	s_2	T_3	0.35	0.35	0.35	0.35	518.60	518.35	6.70	6.70	2.46	2.46	0.01	214.88	227.64
	s_3	T_1	0.34	0.18	0.30	0.09	550.00	544.44	152.81	151.27	54.07	27.19	0.28	232.27	227.56
	s_3	T_2	0.35	0.35	0.35	0.35	518.66	518.66	0.00	0.00	0.00	0.00	0.00	214.62	226.66
	s_3	T_3	0.35	0.09	0.35	0.09	550.00	549.76	6.70	6.70	2.46	0.62	0.01	227.87	227.64
	s_4	T_1	0.17	0.18	0.08	0.09	550.00	544.44	152.81	151.27	26.90	27.19	0.28	222.34	227.56
	s_4	T_2	0.17	0.18	0.08	0.09	550.00	544.65	147.02	145.59	25.48	25.74	0.27	216.98	227.06
	s_4	T_3	0.18	0.18	0.08	0.09	550.00	544.34	155.56	153.96	27.58	27.88	0.28	217.28	228.08
	s_5	T_1	0.09	0.09	0.08	0.09	550.00	549.81	5.23	5.23	0.45	0.48	0.01	219.77	227.13
	s_5	T_2	0.17	0.18	0.08	0.09	550.00	544.65	147.02	145.59	25.48	25.74	0.27	216.98	227.06
	s_5	T_3	0.38	0.18	0.35	0.09	550.00	544.34	155.56	153.96	62.49	27.88	0.28	230.56	228.08
	s_6	T_1	0.18	0.39	0.08	0.35	518.45	512.55	153.01	151.27	28.26	61.40	0.30	209.90	227.56
	s_6	T_2	0.17	0.18	0.08	0.09	550.00	544.65	147.02	145.59	25.48	25.74	0.27	216.98	227.06
	s_6	T_3	0.18	0.18	0.08	0.09	550.00	544.34	155.56	153.96	27.58	27.88	0.28	217.28	228.08
$HVDC_2$	s_1	T_1	0.45	0.30	0.35	0.08	549.63	530.35	529.83	511.25	254.46	158.53	0.96	228.83	223.63
	s_1	T_2	0.26	0.26	0.08	0.10	550.00	536.25	378.06	368.61	98.37	99.34	0.69	215.05	222.37
	s_1	T_3	0.25	0.26	0.08	0.08	549.75	536.32	369.20	360.18	95.07	93.81	0.67	221.26	225.05
	s_2	T_1	0.30	0.30	0.08	0.08	549.63	530.35	529.83	511.25	161.74	158.53	0.96	215.67	223.63
	s_2	T_2	0.26	0.26	0.08	0.10	550.00	536.25	378.06	368.61	98.37	99.34	0.69	215.05	222.37
	s_2	T_3	0.30	0.30	0.08	0.08	548.58	529.34	527.86	509.35	160.93	157.95	0.96	223.53	225.05
	s_3	T_1	0.25	0.26	0.08	0.09	550.00	536.46	372.40	363.23	96.23	96.45	0.68	213.19	223.54
	s_3	T_2	0.43	0.30	0.32	0.08	549.72	530.27	534.69	515.77	243.41	160.63	0.97	228.56	222.37
	s_3	T_3	0.30	0.30	0.08	0.08	548.58	529.34	527.86	509.35	160.93	157.95	0.96	223.53	225.05
	s_4	T_1	0.42	0.26	0.35	0.09	550.00	536.46	372.40	363.23	167.04	96.45	0.68	226.22	223.54
	s_4	T_2	0.32	0.43	0.19	0.35	518.79	504.17	379.30	368.61	125.62	170.32	0.73	206.80	222.37
	s_4	T_3	0.25	0.26	0.08	0.08	549.75	536.32	369.20	360.18	95.07	93.81	0.67	221.26	225.05
	s_5	T_1	0.30	0.30	0.08	0.08	549.63	530.35	529.83	511.25	161.56	158.53	0.96	215.65	223.63
	s_5	T_2	0.41	0.27	0.33	0.11	549.25	535.49	378.08	368.61	163.15	101.42	0.69	226.37	222.37
	s_5	T_3	0.25	0.26	0.08	0.08	549.75	536.32	369.20	360.18	95.07	93.81	0.67	221.26	225.05
	s_6	T_1	0.42	0.26	0.35	0.09	550.00	536.46	372.40	363.23	167.04	96.45	0.68	226.22	223.54
	s_6	T_2	0.26	0.26	0.08	0.10	550.00	536.25	378.06	368.61	98.37	99.34	0.69	215.05	222.37
	s_6	T_3	0.25	0.26	0.08	0.08	549.75	536.32	369.20	360.18	95.07	93.81	0.67	221.26	225.05

TABLE IV
THE WIND POWER GENERATION SCENARIOS AND THEIR ASSOCIATED PROBABILITIES

	wp_s	π_s
s_1	100.00	0.07843
s_2	94.97	0.02500
s_3	84.97	0.03265
s_4	74.98	0.04509
s_5	64.98	0.05011
s_6	54.98	0.07728
s_7	44.99	0.09121
s_8	34.99	0.11222
s_9	19.99	0.10365
s_{10}	15.00	0.11233
s_{11}	5.00	0.06610
s_{12}	0.00	0.20594

variables for the given time horizon.

The proposed approach is implemented on the IEEE 118-bus system to demonstrate its applicability. Two offshore WFs are considered, which are connected to the onshore AC power network through LLC-HVDC links. It is observed from the numerical results that availability of transmission network capacity at the interface of AC/DC networks is a key factor affecting the utilization WF's power generation ability.

APPENDIX A
DATA OF HVDC CONNECTIONS

The data of LLC-HVDC links are given in this appendix, which are derived from [21].

APPENDIX B
WIND GENERATION MODELING [24]

It is assumed that the probability density function (PDF) of wind speed is available in the region under study, then

$$PDF(v) = (\frac{v}{c^2})\ exp[-(\frac{v}{\sqrt{2}c})^2] \tag{39}$$

The probability of falling into scenario s and the corresponding wind speed v_s is calculated as follows:

$$\begin{aligned} \pi_s &= \int_{v_{1,s}}^{v_{2,s}} (\frac{v}{c^2})\ exp[-(\frac{v}{\sqrt{2}c})^2]dv \\ &= exp[-(\frac{v_{1,s}}{\sqrt{2}c})^2] - exp[-(\frac{v_{2,s}}{\sqrt{2}c})^2] \\ v_s &= \frac{v_{2,s}+v_{1,s}}{2} \end{aligned} \tag{40}$$

where $v_{1,s}, v_{2,s}$ are the starting and ending points of the wind speed's interval defined in scenario s, respectively.

The generated power of the wind turbine is determined using its characteristics as follows:

$$P_{wg}(v_s) = \begin{cases} 0 & \text{if } v_s \le v_{in}^c \text{ or } v_s \ge v_{out}^c \\ \frac{v_s - v_{in}^c}{v_{rated} - v_{in}^c} P_{wg}^r & \text{if } v_{in}^c \le v_s \le v_{rated} \\ P_{wg}^r & \text{else} \end{cases} \tag{41}$$

Where, P_{wg}^r is the rated power of wind turbine. The generated power of wind turbine in scenario s is calculated using the obtained v_s and (41).

TABLE V
THE PROBABILISTIC WIND POWER OUTPUTS OF WIND FARMS

Scenario#	Period#	WF-1		WF-2	
		Pw (MW)	Qw (MVAr)	Pw (MW)	Qw (MVAr)
s_1	T_1	5.23	-6.19	529.83	37.37
s_1	T_2	147.02	55.03	378.06	27.44
s_1	T_3	155.56	20.02	369.20	98.50
s_2	T_1	5.23	-4.92	529.83	29.88
s_2	T_2	147.02	68.67	378.06	41.67
s_2	T_3	6.70	0.72	527.86	247.77
s_3	T_1	152.81	31.36	372.40	160.06
s_3	T_2	0.00	40.74	534.69	94.95
s_3	T_3	6.70	41.98	527.86	43.95
s_4	T_1	152.81	70.76	372.40	10.00
s_4	T_2	147.02	-5.91	379.30	195.01
s_4	T_3	155.56	43.74	369.20	6.33
s_5	T_1	5.23	-5.16	529.83	249.74
s_5	T_2	147.02	49.88	378.08	229.38
s_5	T_3	155.56	86.32	369.20	131.34
s_6	T_1	153.01	21.01	372.40	233.69
s_6	T_2	147.02	-5.80	378.06	84.98
s_6	T_3	155.56	-2.04	369.20	90.80
s_7	T_1	4.47	-6.01	449.86	27.44
s_7	T_2	147.02	45.10	378.06	10.68
s_7	T_3	155.56	72.25	369.20	108.41
s_8	T_1	153.83	48.40	349.89	100.43
s_8	T_2	148.72	22.88	349.89	22.24
s_8	T_3	155.91	28.87	349.89	14.13
s_9	T_1	154.70	-5.51	199.94	72.42
s_9	T_2	150.55	-5.78	199.94	39.12
s_9	T_3	154.10	-1.96	199.94	-24.12
s_{10}	T_1	149.95	14.31	149.95	22.36
s_{10}	T_2	149.95	-2.79	149.95	21.88
s_{10}	T_3	149.95	-6.02	149.95	22.86
s_{11}	T_1	49.98	-3.41	49.98	-0.57
s_{11}	T_2	49.98	-242.61	49.98	0.33
s_{11}	T_3	49.98	-0.29	49.98	-0.06
s_{12}	T_1	0.00	0.00	0.00	0.00
s_{12}	T_2	0.00	0.00	0.00	0.00
s_{12}	T_3	0.00	0.00	0.00	0.00

TABLE VI
THE DATA OF STUDIED HVDC LINKS

Parameter	Value	
No. of converters at each side of the HVDC link	2	
No. of 6-pulse bridges at each converter	2	
$R_{L,d}$ (per line)	10Ω	
R_{cr} (per bridge)	6Ω	
R_{ci} (per bridge)	6Ω	
$B_r(=B_i)$	4	
Rated voltage of line to line V_r and V_i	220 kV	
$m=r,i$	min	max
α_m (radian)	0.08	0.35
φ_m (radian)	0	$\pi/2$
$V_{d,m}$ (kV)	450	550
$P_{d,m}$ (MW)	0	1000
T_m	0.3	0.7

REFERENCES

[1] A. Soroudi, "Possibilistic-scenario model for dg impact assessment on distribution networks in an uncertain environment," *IEEE Transactions on Power Systems,*, vol. 27, no. 3, pp. 1283–1293, 2012.

[2] K. Heussen, S. Koch, A. Ulbig, and G. Andersson, "Unified system-level modeling of intermittent renewable energy sources and energy storage for power system operation," *Systems Journal, IEEE*, vol. 6, no. 1, pp. 140 – 151, march 2012.

[3] N. Alguacil and A. Conejo, "Multiperiod optimal power flow using benders decomposition," *IEEE Transactions on Power Systems,*, vol. 15, no. 1, pp. 196 –201, feb 2000.

[4] T. Amraee, A. Ranjbar, B. Mozafari, and N. Sadati, "An enhanced under-voltage load-shedding scheme to provide voltage stability," *Electric Power Systems Research*, vol. 77, no. 8, pp. 1038 – 1046, 2007.

[5] N. Alguacil and A. Conejo, "Multiperiod optimal power flow using benders decomposition," *IEEE Transactions on Power Systems,*, vol. 15, no. 1, pp. 196–201, 2000.

[6] M. Montilla-DJesus, D. Santos-Martin, S. Arnaltes, and E. Castronuovo, "Optimal operation of offshore wind farms with line-commutated hvdc link connection," *IEEE Transactions on Energy Conversion*, vol. 25, no. 2, pp. 504 –513, june 2010.

[7] J. Arrillaga, Y. Liu, and N. Watson, *Front Matter*. Wiley & Sons Ltd, 2007.

[8] B. Franken and G. Andersson, "Analysis of hvdc converters connected to weak ac systems," *IEEE Transactions on Power Systems,*, vol. 5, no. 1, pp. 235–242, 1990.

[9] L. Shi, C. Wang, L. Yao, Y. Ni, and M. Bazargan, "Optimal power flow solution incorporating wind power," *Systems Journal, IEEE*, vol. 6, no. 2, pp. 233–241, 2012.

[10] R. Jabr and B. Pal, "Intermittent wind generation in optimal power flow dispatching," *Generation, Transmission & Distribution, IET*, vol. 3, no. 1, pp. 66–74, 2009.

[11] P. Yu and B. Venkatesh, "A practical real-time opf method using new triangular approximate model of wind electric generators," *IEEE Transactions on Power Systems,*, vol. to appear, 2012.

[12] M. Montilla-DJesus, D. Santos-Martin, S. Arnaltes, and E. Castronuovo, "Optimal reactive power allocation in an offshore wind farms with lcc-hvdc link connection," *Renewable Energy*, 2011.

[13] A. Tapia, G. Tapia, and J. Ostolaza, "Reactive power control of wind farms for voltage control applications," *Renewable Energy*, vol. 29, no. 3, pp. 377 – 392, 2004.

[14] T. Amraee, A. Soroudi, and A. Ranjbar, "Probabilistic determination of pilot points for zonal voltage control," *Generation, Transmission & Distribution, IET*, vol. 6, no. 1, pp. 1–10, 2012.

[15] Y. Atwa and E. El-Saadany, "Probabilistic approach for optimal allocation of wind-based distributed generation in distribution systems," *Renewable Power Generation, IET*, vol. 5, no. 1, pp. 79 –88, 2011.

[16] X. Liu, "Economic load dispatch constrained by wind power availability: A wait-and-see approach," *Smart Grid, IEEE Transactions on*, vol. 1, no. 3, pp. 347–355, 2010.

[17] D. Santos-Martin, S. Arnaltes, and J. R. Amenedo, "Reactive power capability of doubly fed asynchronous generators," *Electric Power Systems Research*, vol. 78, no. 11, pp. 1837 – 1840, 2008.

[18] Y. Atwa, E. El-Saadany, M. Salama, and R. Seethapathy, "Optimal renewable resources mix for distribution system energy loss minimization," *IEEE Transactions on Power Systems,*, vol. 25, no. 1, pp. 360 –370, feb. 2010.

[19] B. Mohammadi-ivatloo, A. Rabiee, and M. Ehsan, "Time-varying acceleration coefficients ipso for solving dynamic economic dispatch with non-smooth cost function," *Energy Conversion and Management*, vol. 56, no. 0, pp. 175 – 183, 2012.

[20] A. J. 2010, "http://www.pserc.cornell.edu/matpower."

[21] P. Kundur, *Power system stability and control*. McGraw-hill New York, 1994.

[22] A. Brook, D. Kendrick, and A. Meeraus, "Gams, a user's guide," *ACM SIGNUM Newsletter*, vol. 23, no. 3-4, pp. 10–11, 1988.

[23] A. J. 2012, "www.gams.com/dd/docs/solvers/conopt.pdf."

[24] A. Soroudi and M. Afrasiab, "Binary pso-based dynamic multi-objective model for distributed generation planning under uncertainty," *Renewable Power Generation, IET*, vol. 6, no. 2, pp. 67 –78, march 2012.